European Commission
Research Programme of the Research Fund for Coal and Steel

INNOSEIS

Valorization of innovative anti-seismic devices

WORK PACKAGE 2 – DELIVERABLE D2.1

Recommended procedure for EN1998-compatible behaviour factor evaluation of new structural systems

Coordinator:

National Technical University of Athens - NTUA, Greece

Beneficiaries:

Universitatea Politehnica Timisoara - UPT, Romania

Politecnico di Milano - POLIMI, Italy

Universita Degli Studi di Napoli Federico II - UNINA, Italy

Universita di Pisa - UNIPI, Italy

Rheinisch-Westfaelische Technische Hochschule Aachen - RWTH, Germany

Instituto Superior Tecnico - IST, Portugal

Universitet po Architektura Stroitelstvo i Geodezija - UACEG, Bulgaria

Universiteit Hasselt - UHasselt, Belgium

Maurer Sohne Engineering GmbH & CO KG - MSE, Germany

Convention Europeenne de la Construction Metallique ASBL - ECCS, Belgium

Grant Agreement Number: 709434

01/09/2017

AUTHORS:

NATIONAL TECHNICAL UNIVERSITY OF ATHENS
Institute of Steel Structures
15780 Athens, Greece
Authors: Dimitrios Vamvatsikos, Konstantinos Bakalis, Mohsen Kohrangi, Pavlos Thanopoulos, Ioannis Vayas

POLITECNICO DI MILANO
Department of Architecture, Built Environment and Construction Engineering
Piazza Leonardo da Vinci, 32, 20133 Milan, Italy
Authors: Carlo Castiglioni, Alper Kanyilmaz

UNIVERSITA DEGLI STUDI DI NAPOLI "FEDERICO II"
Department of Structures for Engineering and Architecture
Via Forno Vecchio 36, Napoli, 80134, Italy
Authors: Mario D' Aniello

UNIVERSITEIT HASSELT
Faculty of Engineering Technology
Agoralaan, Gebouw H, Diepenbeek 3590, Belgium
Authors: Hervé Degee

RHEINISCH-WESTFAELISCHE TECHNISCHE HOCHSCHULE AACHEN
Institute of Steel Construction
Mies-van-der-Rohe Str. 1, 52074 Aachen
Authors: Benno Hoffmeister, Marius Pinkawa

UNIVERSITA DI PISA
Department of Civil and Industrial Engineering,
Largo Lucio Lazzarino 1, 56122, Pisa, Italy
Authors: Francesco Morelli

POLITEHNICA UNIVERSITY OF TIMISOARA
Department of Steel Structures and Structural Mechanics
Ioan Curea Street, no.1, Timisoara, Romania
Authors: Aurel Stratan

INSTITUTO SUPERIOR TECNICO
Department of Civil Engineering, Architecture and Georesources
Av. Rovisco Pais, 1049-001 Lisbon, Portugal
Authors: Luís Calado, Jorge M. Proença

UNIVERSITET PO ARCHITEKTURA STROITELSTVO I GEODEZIJA
Department of Steel and Timber Structures
1 Hr. Smirnenski blvd. 1046 Sofia, Bulgaria
Authors: Tzvetan Georgiev

TABLE OF CONTENTS

1 Introduction

The application of linear design procedures for seismic loading is based on the approximation of the nonlinear dynamic response of the structure via a linear model. To account for the beneficial effects of ductility, which allows trading off damage for lower design forces, EN 1998-1 [1] adopts the behaviour factor to divide the elastic design response spectrum. Still, EN 1998-1 only provides values of the q-factor for a very limited number of systems. In order to introduce new and innovative lateral load resisting systems into the code, researchers have at times proposed q-values, yet without much consensus: Each proposal comes with its own definition of a safety target and seismic performance assessment method, the latter often reflecting the limited resources available to the researchers. Overall, this uneven process lends little confidence to the proposed q-factors, vis-à-vis the target of achieving a uniform risk level across different systems and sites in Europe. Unlike in the US, where the well-received FEMA P-695 [2] standard has largely settled this debate, Europe has not formulated a standard methodology to define and validate the q-factors. As a direct remedy, the recent EU-funded INNOSEIS project is offering a novel procedure for obtaining consistent values for q based on the definition of a set of structures to represent each class of buildings, the use of nonlinear static and dynamic analysis methods and the incorporation of the effect of aleatory and epistemic uncertainty on the actual systems' performance to reach a uniform level of safety across the entire building population.

2 Proposed approach

The proposed q-factor estimation methodology is based on the explicit performance assessment of a number of archetype structures using two performance targets defined on a mean annual frequency of exceedance basis. It comprises seven discrete steps, taking the engineer from the site hazard to the final risk-based determination of compliance with the safety standards.

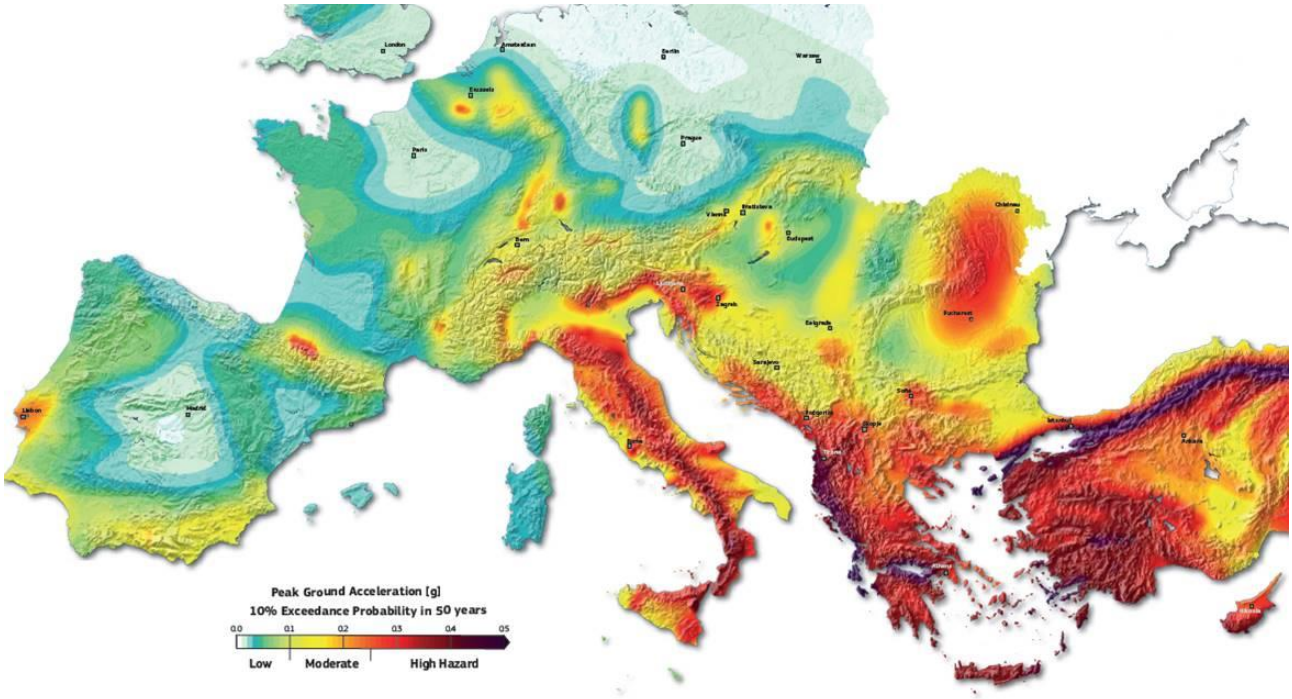

Figure 2-1: Peak ground acceleration with a 10% in 50 years exceedance probability according to the EU-SHARE model [3] **(adapted from www.efehr.org).**

2.1 Step 1: Site Hazard

To appropriately capture the seismicity across a wide swath of Europe, two different sets of 3 sites are considered. The first set comprises moderate seismicity sites with a peak ground acceleration (or zone factor per EN1998) of approximately a_g = 0.15g, mainly geared towards evaluating behaviour factors for Ductility Class Medium (DCM) designs. The second set uses high-seismicity sites with a_g = 0.30g that can be employed to test Ductility Class High (DCH) buildings. A single rock soil type is considered, having a shear wave speed in the upper 30m of v_{s30} = 800m/s, making it borderline soil type B per EN1998. Additional soil types may be of interest for a more comprehensive evaluation. Site selection was performed according to the EU-SHARE seismicity model [3] by matching the required value of a_g to the peak ground acceleration with a 10% in 50yrs probability of exceedance (Figure 2-1), while seeking to distribute the sites as evenly as possible across the map of Europe. The resulting sites appear in the map of Figure 2-2, with their geographical coordinates shown in Table 2-1 and Table 2-2 for moderate and high seismicity, respectively.

For each site all sources within 200km were considered using the area source model of EU-SHARE. The corresponding seismic hazard curves were computed for each site for the intensity measure (IM) of *AvgSa* (Figure 2-3). *AvgSa* [4–6] is a modern IM that comprises the geometric mean of 5% damped spectral acceleration ordinates S_a at periods T_{Ri} characterizing the archetype buildings of interest:

$$AvgSa\left(T_{Ri}\right)=\left(\prod_{i=1}^{n} S_a\left(T_{Ri}\right)\right)^{1/n} \quad (2–1)$$

Each S_a value in Equation (2–1) is actually the geometric mean of both horizontal components, rather than an arbitrary selection of one of the two. Generally speaking, periods T_{Ri} can be selected as linearly spaced within a range of $[T_L,T_H]$, where T_L is a low period near the minimum second mode of the buildings to be investigated and T_H is a high period that is near 1.5 times their maximum first mode period. If considerable difference exists among the different first mode periods, one should consider using two different definitions of *AvgSa*, one for low/mid-rise structures (shorter periods) and another for high-rise ones (longer periods), for better fidelity. Herein, for reasons of simplicity we employed a single period range for all types of structures of [0.3s, 3.0s] with an increment of 0.2s.

For each site, the value of *AvgSa* was estimated that corresponds to an exceedance probability of 2% in 50 years, or equivalently to a mean annual frequency (MAF), or mean annual rate (MAR) of $-\ln(1-0.02)/50 = 0.000404$. At this intensity level disaggregation analysis was performed to find the contributions from different magnitude (M), distance (R) and epsilon (ε) bins to the hazard, as shown in detail in Figure 2-4. The corresponding mean magnitude, $\overline{M}$, distance, $\overline{R}$, and epsilon, $\overline{\varepsilon}$ of all the scenarios appear in Table 2-3. Then, the multi-site Conditional Spectrum record selection approach [7–10] was employed on the basis of *AvgSa* to select two sets of 30 ordinary (not pulse-like, not long duration) recordings that are appropriate for the 2% in 50yrs level of intensity; one set for all medium seismicity sites and another for all high-seismicity ones, both available online [11,12]. Their spectra and the corresponding minor discrepancies achieved vis-à-vis the conditional mean and standard deviation targets appear in Figure 2-5, Figure 2-6 for medium seismicity, and Figure 2-7, Figure 2-8 for high-seismicity. These ground motions will be employed for performing dynamic analysis in Section 2.5 (Step 5).

Further pan-European verification of q-factors for final inclusion in the code will likely require additional record sets that incorporate near-source directivity pulses or long-duration subduction zone motions. Assembling such motions is a process that may be strongly site-dependent and will complicate the assessment process needlessly at this level. Still, it should remain as an important consideration for future improvements.

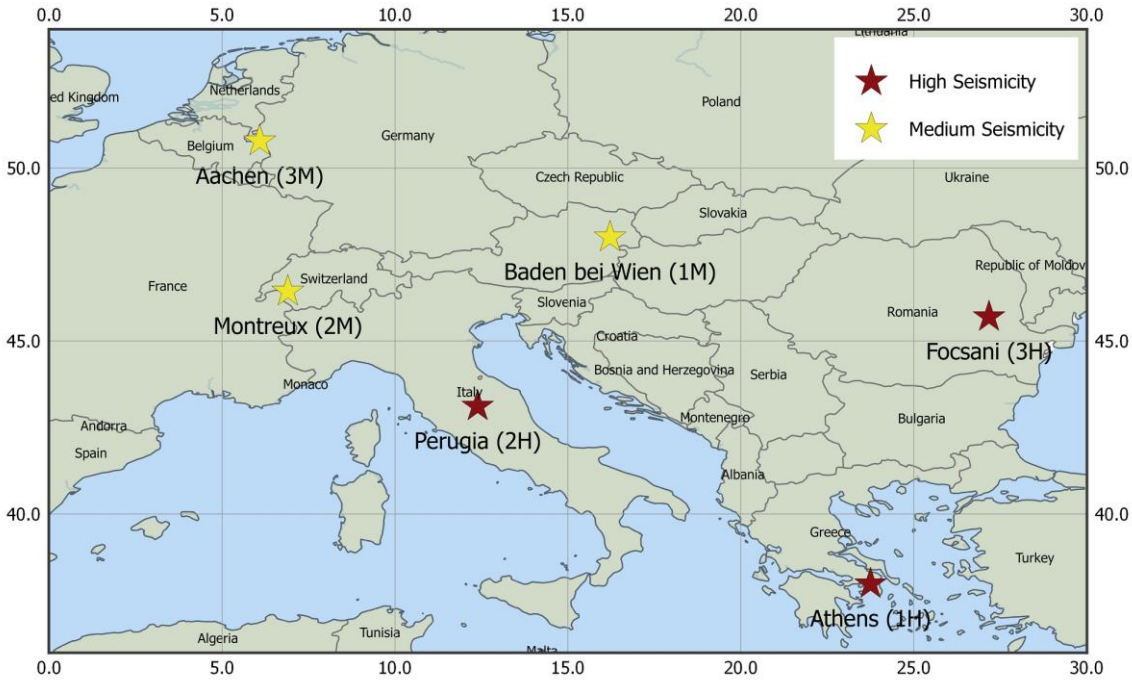

Figure 2-2: Selected European sites of medium and high seismicity.

Table 2-1: Coordinates of medium seismicity sites

ag ≈ 0.15g	Baden bei Wien	Montreux	Aachen
Latitude	47.999	46.433	50.776
Longitude	16.218	6.899	6.085

Table 2-2: Coordinates of high seismicity sites

ag ≈ 0.30g	Athens	Perugia	Focșani
Latitude	37.976	43.111	45.696
Longitude	23.751	12.389	27.179

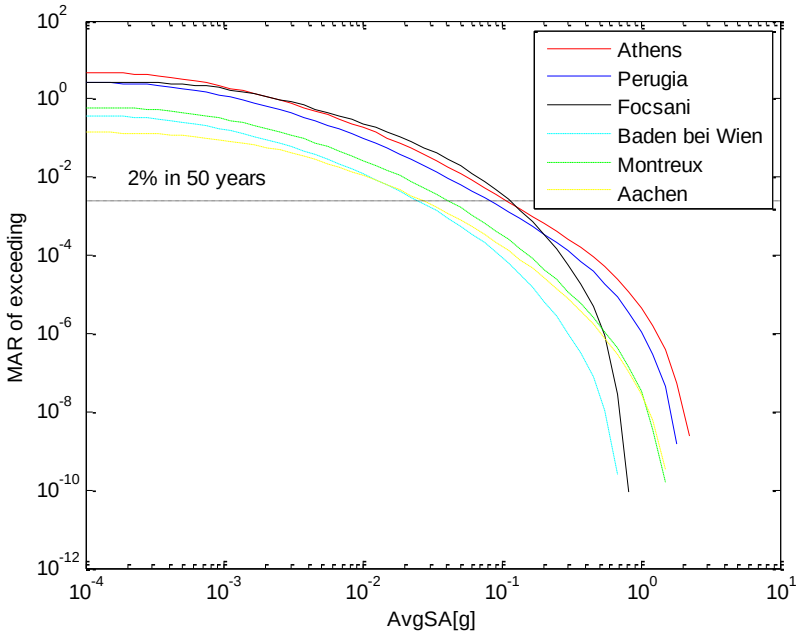

Figure 2-3: Hazard curves for the six European sites for *AvgSa* with a period range of [0.3s, 3.0s] and an increment of 0.2s

Table 2-3: Disaggregation statistics at the 2% in 50yrs probability of exceedance level, in terms of the mean magnitude (M_bar), the mean distance (R_bar), and the mean deviation from the ground motion prediction equation mean estimate (Eps_bar).

	AvgSA [g] 2% in 50 years	M_bar	R_bar [km]	Eps_bar
Athens	0.107	7.03	23.30	1.21
Perugia	0.082	6.74	18.55	1.11
Focsani	0.113	6.99	29.88	1.56
Baden bei Wien	0.025	6.02	35.23	0.95
Montreux	0.041	6.40	35.03	1.11
Aachen	0.027	6.12	27.13	0.95

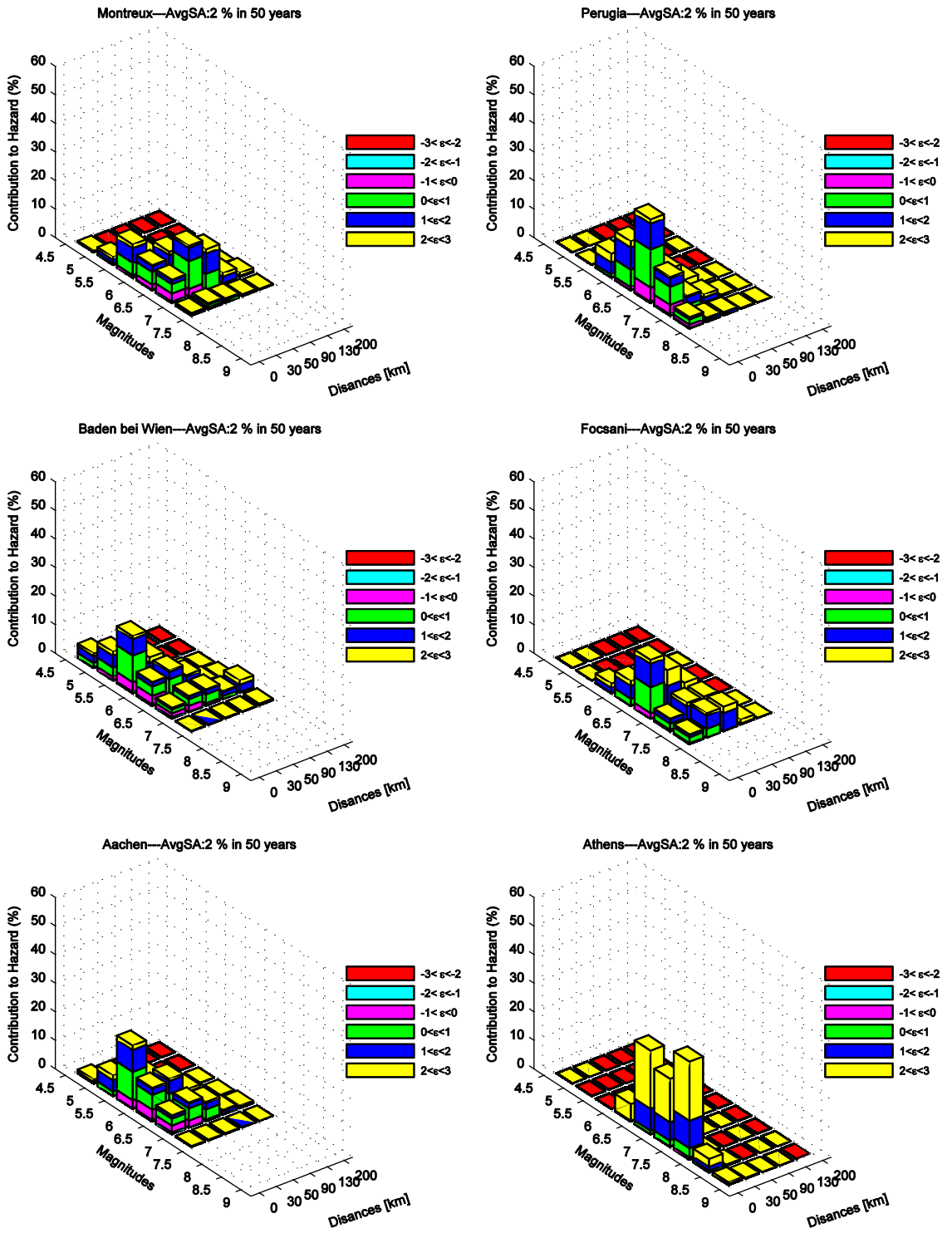

Figure 2-4: Hazard disaggregation results for the three medium-seismicity (left) and the three high seismicity (right) European sites in magnitude and distance bins for the 2% in 50yrs exceedance probability level.

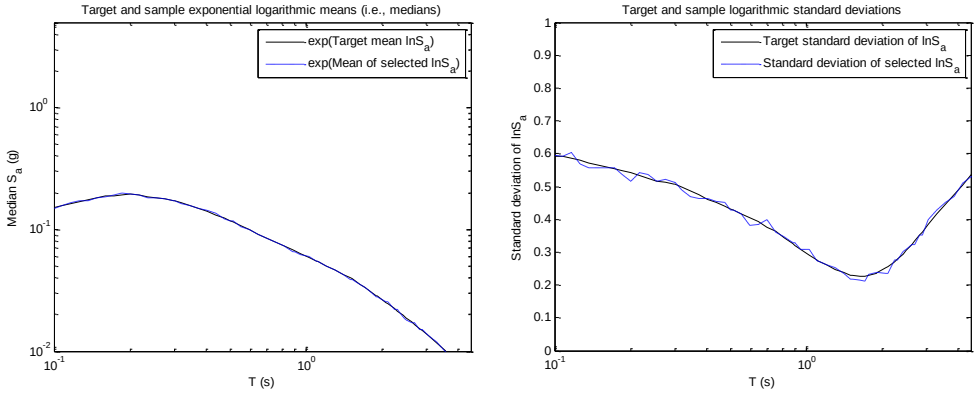

Figure 2-5: Spectral target matching for medium seismicity sites: (a) exponential logarithmic mean and (b) logarithmic standard deviation.

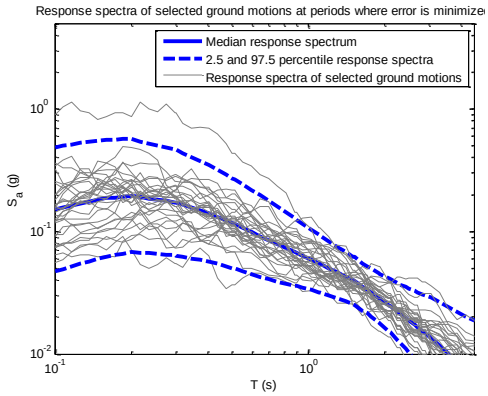

Figure 2-6: Response spectra of selected ground motions for medium seismicity sites (2% in 50yrs level).

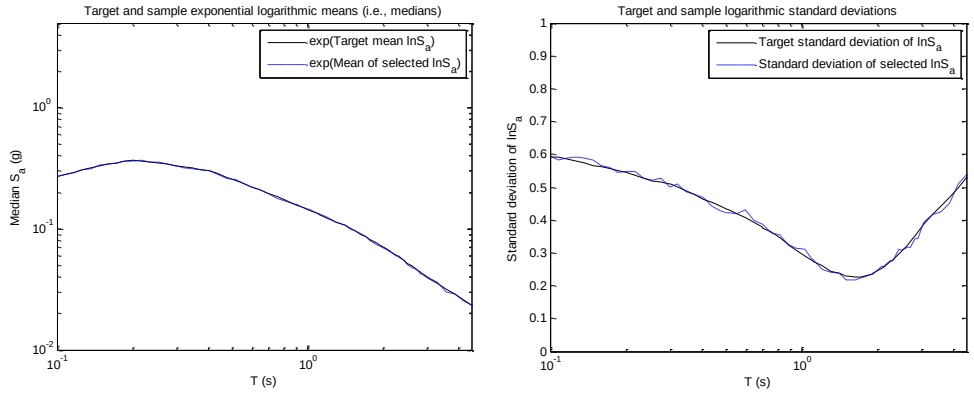

Figure 2-7: Spectral target matching for high seismicity sites: (a) exponential logarithmic mean and (b) logarithmic standard deviation.

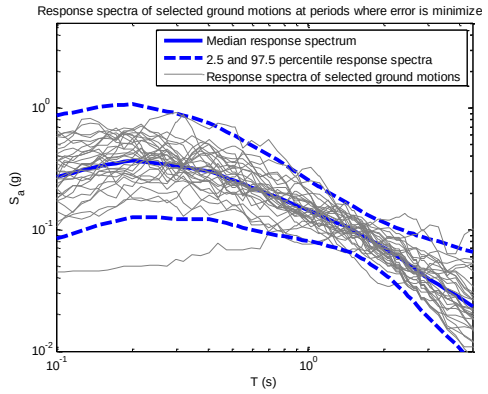

Figure 2-8: Response spectra of selected ground motions for high seismicity sites (2% in 50yrs level).

2.2 Step 2: Archetype Buildings

In a comprehensive study, numerous archetype buildings need to be selected, representing a wide range of potential combinations of influential structural characteristics, such as the number of stories/bays, story height, bay width, degree of vertical irregularity etc. Generally, the use of more buildings highly improves the fidelity of the approach, essentially needing at least 12-20 buildings to have reasonable confidence in the q-factor estimates obtained. Still, for the pre-normative assessment to be conducted herein, three archetype configurations have been selected. They are vertically regular, square-plan, residential/office buildings of typical dimensions for steel structures (Figure 2-9): A low-rise (2-story), a mid-rise (4-story) and one high-rise (8-story), the latter only for systems that are applicable to tall buildings (Figure 2-10). Each building shall be designed according to EN1993/EN1998 [1,13] and according to the design guide for the lateral-load-resisting system to be investigated, using the recommended values (rather than any specific country's) for nationally determined parameters. As an initial q-factor for design, one may use either existing estimates from previous research or a trial value of 3 – 6 based on engineering judgment.

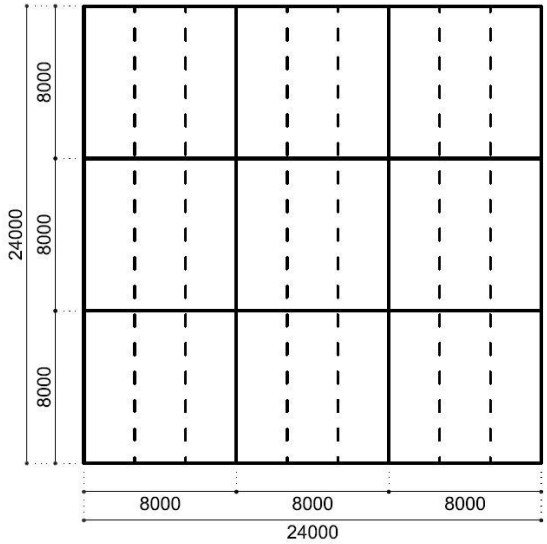

Figure 2-9: Plan-view of the 2/4/8-story archetype structures (dimensions in mm)

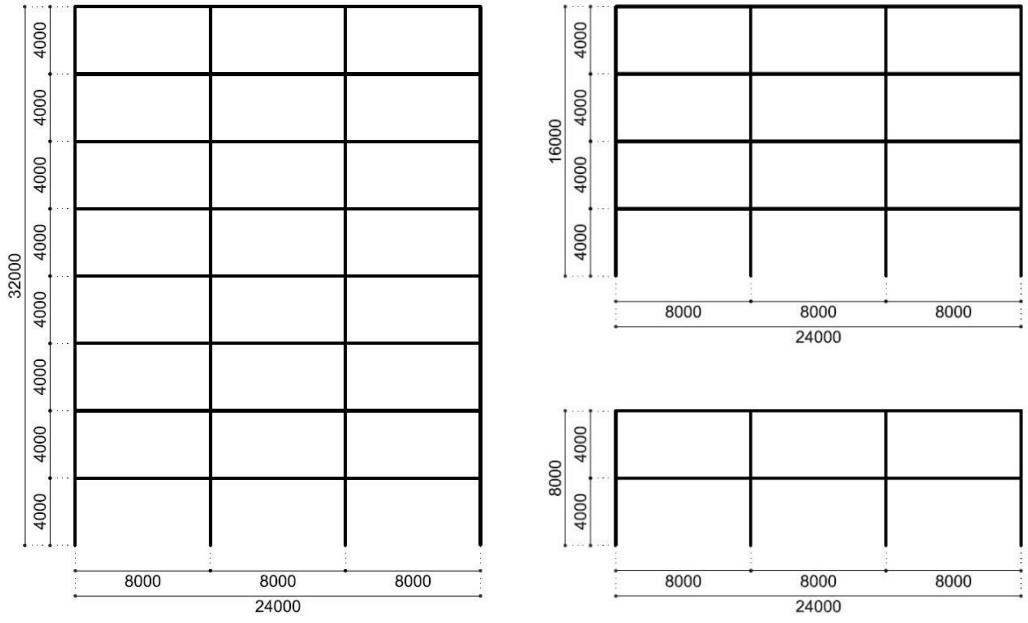

Figure 2-10: Side-view of the 2/4/8-story archetype structures (dimensions in mm)

In general, as different q-factors are stipulated for each ductility class of EN1998 [1], two versions of each archetype building should be created to be able to determine at least DCM and DCH values: One for a_g = 0.30g for DCH requirements and another for a_g = 0.15g for DCM. In cases where only one ductility class is of interest, or if the system under consideration is only meant to be used for one of these two site/ductility combinations, assessment and design can be appropriately curtailed.

2.3 Step 3: Nonlinear Models

A nonlinear model of the structural system of each archetype building realization is created. 3D models are preferable if, for example, plan asymmetry or biaxial loading are present. Otherwise, experience has shown that 2D models are preferable, as they can offer faster and more reliable convergence, especially in the region of global collapse, offering accuracy without a heavy computational burden. The model should incorporate accurate hysteresis, including both in-cycle and cyclic degradation, of all system components that may enter the nonlinear range. Optimally, component modelling should be able to accurately reproduce both the monotonic (with in-cycle degradation) and the hysteretic (with cyclic degradation) performance of these elements. Each nonlinear element should also be able to display a clearly defined fracturing deformation (drift, rotation, strain or displacement) whereby it loses all strength and stiffness and ceases to function. Figure 2-11 presents the minimum backbone information each nonlinear element should display. The mass and stiffness of secondary structural and non-structural elements should be incorporated according to state-of-practice approaches, e.g. via a leaning P-Δ column or an adjacent full gravity frame.

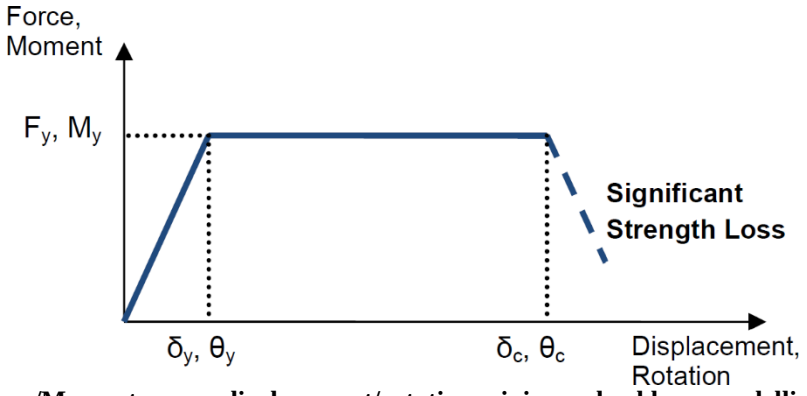

Figure 2-11: Force/Moment versus displacement/rotation minimum backbone modelling requirements

2.4 Step 4: Static Analysis

Nonlinear static pushover analysis shall be performed for each archetype. A preliminary q-factor will be established from the analysis, using the classic product of overstrength Ω and ductility behaviour factor q_d:

$$q_{stat} = q_d \cdot \Omega = \frac{\delta_{0.2}}{\delta_y} \cdot \frac{a_u}{a_1} \qquad (2\text{–}2)$$

For compatibility with EN1998 [1], overstrength is defined as a_u/a_1, i.e., the ratio of the maximum base shear strength over the base shear at first yield. The latter is the base shear corresponding to the first plastification of any single sacrificial ("dissipative") element in the structure. The ductility behaviour factor may be defined as the ratio of the roof displacement at 20% loss of maximum strength, $\delta_{0.2}$, and the yield displacement, δ_y, whereby we are implicitly assuming the equal displacement rule holds. Figure 2-12 shows how such quantities may be located on the pushover curve.

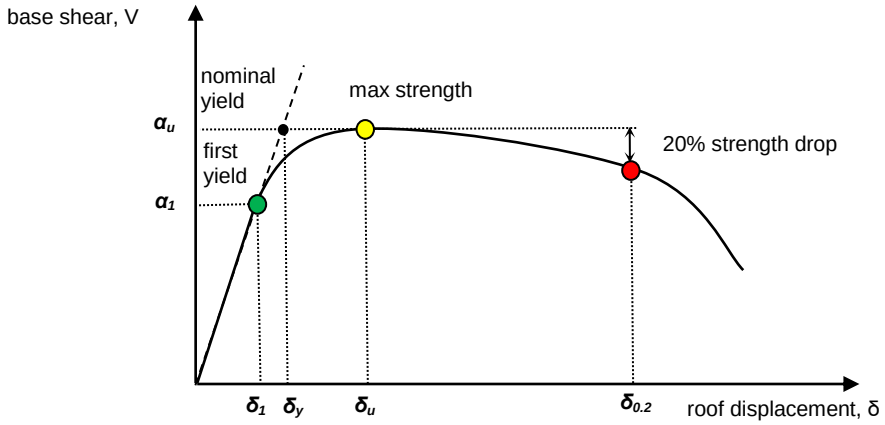

Figure 2-12: Example of q-factor determination on a static pushover capacity curve.

Note that the Ω definition conservatively neglects the overstrength provided by oversizing of members, which is taken into account by US codes and incorporated into the FEMA P-695 [2] standard. If the estimated q_{stat} factor is found to be more significantly different from the one originally assumed for design for any of the archetypes (Step 2), then the initial trial value of q adopted may need to be adjusted and a redesign is required. Still, behaviour factor values obtained via the static approach should only be considered as indicative since they are often found to be less accurate than those estimated via the dynamic approach introduced in the following. The one value that will be of certain use from this step is the overstrength Ω, as it can be employed in the code to offer some flexibility in the definition of the q-factor, as presently done by EN1998 [1].

2.5 Step 5: Dynamic Analysis

Each archetype is subjected to the set of records selected for the peak ground acceleration value used for its design. Incremental Dynamic Analysis (IDA) [14] is employed, covering the entire post-yield range of response all the way to the first appearance of global collapse in a building, either as global dynamic instability due to simulated modes of failure, or in the form of non-simulated modes of failure introduced in post-processing. Figure 2-13 shows an example of IDA for a 12-story. For each archetype, the results are evaluated using *AvgSa* [6,15] as the *IM*, i.e., the geometric mean of multiple S_a ordinates evenly spaced within the period range of interest as defined in Equation (2–1).

When there is considerable variation in first-mode periods across the class, it becomes more efficient to define *AvgSa* by employing S_a ordinates linearly spaced within the range of $[T_2, 1.5T_1]$, where T_1 and T_2 are the first and second mode of each system investigated. This definition may provide improved results, i.e., lower dispersions and thus better predictive ability, but it also requires a separate estimation of the hazard curve and perhaps even a separate record selection for each building, therefore it will severely complicate the hazard and performance assessment process. For simplicity, we shall employ the more general definition of the range of periods used in Step 1 that cover all building archetypes defined in Step 2.

From each dynamic analysis all needed engineering demand parameters (EDPs) should be recorded, including both sacrificial (ductile) and non-sacrificial (brittle) elements that may enter the nonlinear range and/or participate in failure mechanisms. Failure of non-sacrificial elements is often not included in the model, thus it may need to be incorporated as a non-simulated mode of failure in post-processing. Conservatively, this may mean that global collapse is taken to occur at the first occurrence of such a failure mode.

Finally, particular attention needs to be paid to the capability of the model to undergo large deformations, in line with experimental results, before non-convergence occurs. Commercial software models are often unable to follow the deformations of components deep in the post-yield range (especially in negative stiffness), often failing to converge when the first few sacrificial

elements have fractured. Correspondingly, the estimated collapse capacity is severely curtailed.

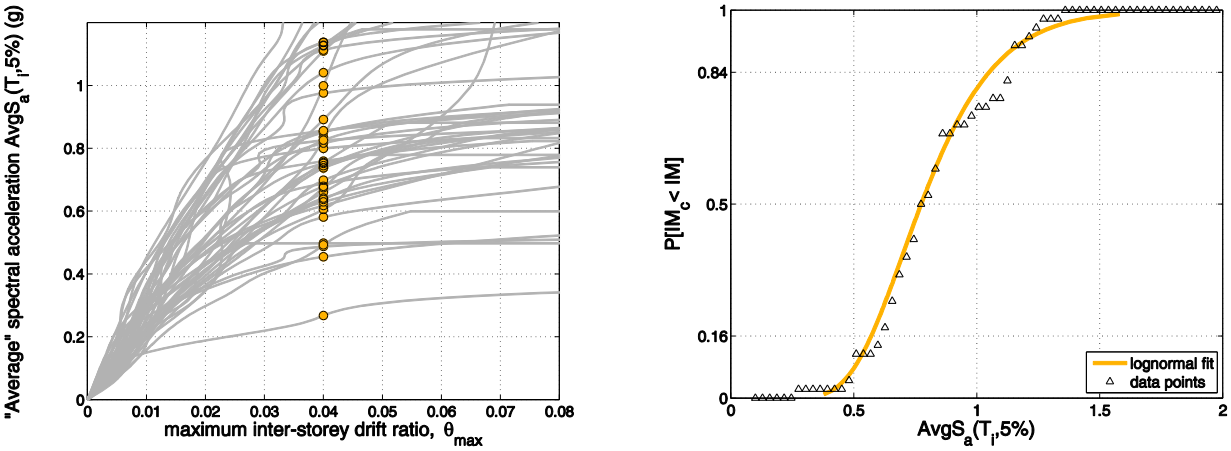

(a) (b)

Figure 2-13: (a) 44 IDA curves for a 12-story index buildings and a "vertical stripe" of *IM*=AvgS_a "capacity values" at an inter-story drift level of 4%. (b) Fragility curve.

2.6 Step 6: Performance Criteria and Fragility Assessment

Each archetype's performance is verified against two performance objectives, namely Life Safety (LS) and Global Collapse (GC). LS is checked against a mean annual frequency of 10% in 50 years, while GC for the 1 or 2% in 50 years value. The exact values to be used in a normative assessment should be calibrated to ensure maximum compatibility with existing EN1998 designs.

In general, two types of checks are used in performance assessment. Strength checks are employed to verify that no potential structural element enters a brittle mode of failure (e.g., lateral-torsional buckling). These can often be deemed to be satisfied automatically thanks to capacity design, although checking whether this is indeed the case at each step of the dynamic analysis makes for a holistic "design approach" verification, beyond just deriving a value for q. For ductile modes of failure, deformation checks are applied to verify that no sacrificial (or "energy dissipating") structural element exceeds its plastic deformation capacity.

For LS checking, the approach developed by Vulcu et al. [16] was adopted for deriving acceptance criteria. It is based on provisions of EN 1998-1 [1], ASCE41-13 [17] and FEMA P-795 [18]. First, the seismic performance of the sacrificial components is assessed by identifying component deformation corresponding to two component-specific performance levels, namely significant damage (SD), and near collapse (NC), assumed to be characterized by the following description (based on FEMA 356 [19]):

- *Significant Damage:* Significant damage, with some margin against total collapse of the component
- *Near Collapse:* Heavy damage, with low residual strength and stiffness of the component.

Backbone curves are first constructed for each sacrificial element, for example based on the provisions from FEMA P-795 for cyclic moment-rotation or force-deformation data. In a second step, the rotations/deformations corresponding to the two performance levels are identified. The rotation related to the Significant Damage performance level is considered as corresponding to the drop of force/moment by 20% relative to the maximum value attained, but not more than 0.75 times the deformation at Near Collapse. The deformation associated with the Near Collapse performance level, is considered as corresponding to a drop of force/moment by 80% from its maximum value, but not more than the maximum deformation attained during the test (Figure 2-14). It is deemed that Life Safety is violated when the first sacrificial element reaches its SD limit-state. Obviously, it is also expected that all non-sacrificial structural elements should remain without any damage.

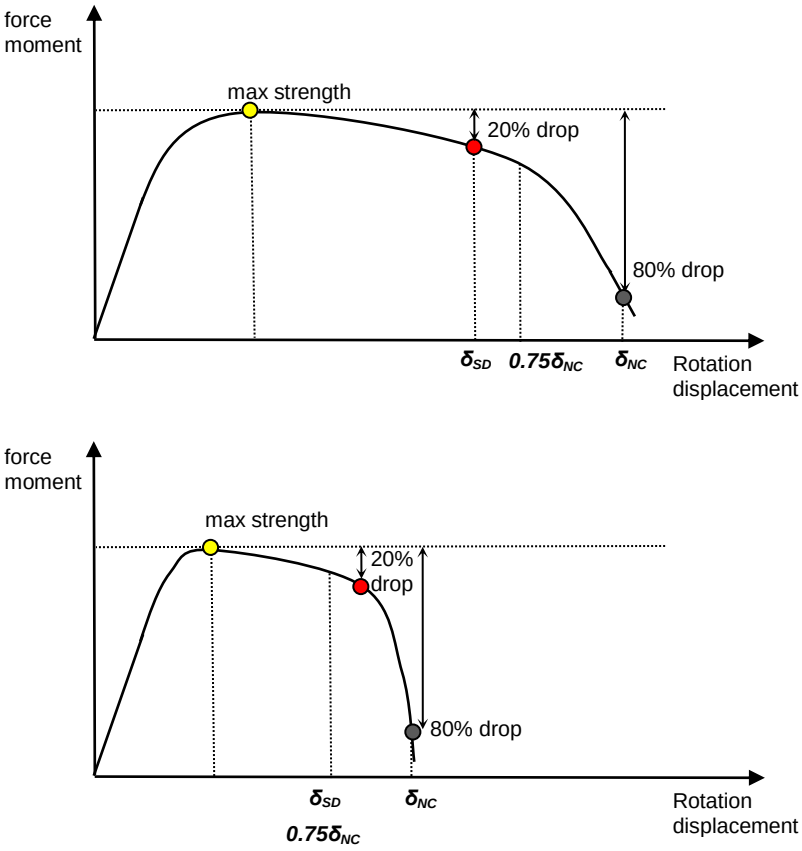

Figure 2-14: Two examples of SD definition on a component capacity curve. For a component with low in-cycle degradation (top), the SD limit-state is defined by the 20% loss of strength. For a component that rapidly loses strength, (bottom), SD is defined by 75% of the NC state deformation.

GC checking is considered as a numerically more challenging task and it requires a robust model that is capable of following the behaviour of the building all the way to global collapse. Optimally, this will be performed by checking only for simulated modes of failure, typically ductile modes of failure that are explicitly incorporated in the model. In case capacity design is not guaranteed to prevent the appearance of brittle modes of failure, something that may occur after some sacrificial elements have reached their ultimate fracture ductility and ceased to offer strength or stiffness to the building, then non-simulated modes of failure may also be introduced in postprocessing of the results. In all cases, a single global collapse point is established in each individual IDA curve, using the flatline for simulated modes (Figure 2-13(a)) and the earliest occurring non-simulated mode, whichever comes first. The ensemble of all global collapse points can be fitted to determine the GC fragility function. In cases where the model is not capable of displaying global collapse, a more conservative check may be performed for ductile modes of failure, whereby global collapse shall be assumed to occur when the first ductile element reaches its ultimate (fracturing) deformation. Still this will certainly curtail the attainable value of q.

2.7 Step 7: Acceptance or rejection of q-factor

Performance verification will be performed according to the Cornell et al. [20] fragility-hazard convolution approach (Figure 2-15) to determine $\lambda(DS)$, i.e., the mean annual frequency (MAF) of exceeding the damage state (*DS*, being either LS or GC) of interest:

$$\lambda(DS) = \int_{IM} \mathrm{P}[D > C|IM] \left| \mathrm{d}\lambda(IM) \right| \tag{2–3}$$

$\lambda(IM)$ is the MAF of exceeding values of the *IM*, i.e., the hazard curve derived in Step 1 for the intensity measure, *IM*, of *AvgSa*. $P[D>C|\mathrm{IM}]$ is the fragility function, providing the conditional probability of violating DS by checking demand *D*, estimated from dynamic analyses in Step 5, against the DS capacity *C* given the *IM* level. Both *D* and *C* are expressed in terms of an engineering demand parameter (EDP), i.e., a response parameter that can be used to determine exceedance of the *DS*. For GC this is always the maximum interstory drift, considering all stories, while for LS it is usually the response parameter that best expresses the exceedance of SD (see Step 6) by the first sacrificial element in the building. This can also be a maximum interstory drift variable if reliable means are found to relate its values with the failure of the element in question.

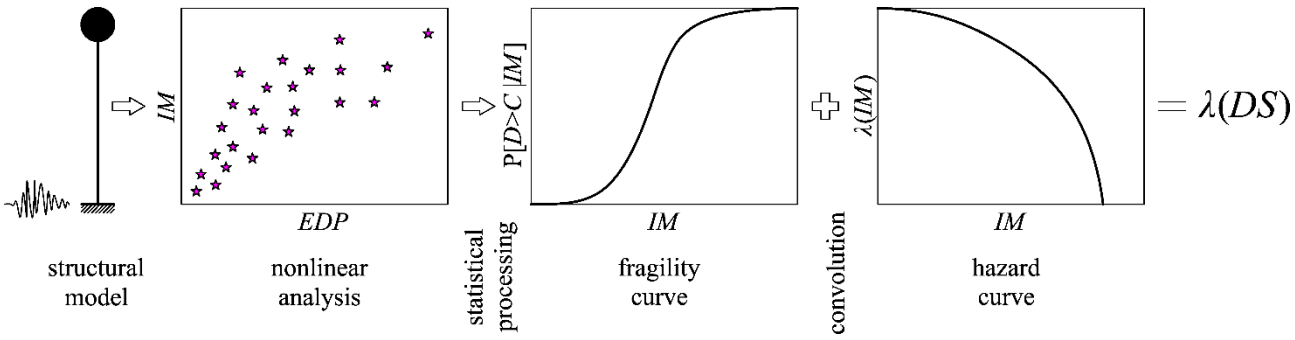

Figure 2-15: The concept of performance assessment according for a given damage state (DS), by extracting the fragility curve from nonlinear dynamic analyses and convolving with the hazard curve over all values of the IM.

There are considerable uncertainties that need to go into the estimation of $\lambda(DS)$ via Equation (2–3). Comprehensively taking them into account is no simple task. Even if we assume that the use of the mean hazard adequately takes into account the uncertainty inherent in the hazard assessment itself (Cornell et al. [20]), there are considerable demand and capacity uncertainties derived from modeling, analysis, sample, element tests and even the archetype sample size employed. For simplicity, under a lognormal distribution assumption, it is typical to estimate the overall dispersion (logarithmic standard deviation) for *DS* due to uncertainty, β_{DSU}, as the square-root-sum-of-squares of the individual components:

$$\beta_{DSU} = \sqrt{\beta_{TD}^2 + \beta_{DR}^2 + \beta_C^2} \tag{2–4}$$

The dispersions combined are: β_{TD} due to test data quality rating, β_{DR} due to design rules quality rating, and β_C due to DS capacity dispersion. β_{TD} and β_{DR} are based on expert opinion. Where no further guidance is available, one may use pertinent values from FEMA P-695 [2]. Therein, values of 0.50, 0.35, 0.20 and 0.10 are suggested for Poor, Fair, Good and Superior ratings and for GC assessment. For β_C one should employ the natural dispersion observed in tests of the sacrificial element type if LS is tested, while for GC one should use a value that conveys the uncertainty in the assessment of collapse given the maximum interstory drift. Some guidance on selecting dispersion values may also be found in FEMA P-58 [21]. In general, though, one should take care to use lower β_{DSU} for LS than for GC, reflecting the higher uncertainty associated with collapse. As a general rule of thumb, β_{LSU} can be assumed to be 25% lower than $\beta_{GCU.}$

To take into account the epistemic uncertainties in assessment, we define an *x*% level of confidence vis-à-vis epistemic uncertainties and assess the *x*% value of the MAF. This is essentially the MAF value with an x% probability of not being exceeded due to uncertainty. Its estimation can be performed either in an accurate numerical approach or with an analytical approximation. The latter case is the easiest to implement, but at the same time it lacks in accuracy. Its basis is the Cornell et al. [16] approximation, whereby Equation (2–3) can be written as:

$$\lambda(DS) \approx \lambda(IM_{C50\%}) \exp\left(0.5k^2 \beta_{DSR}^2\right) \quad (2–5)$$

where, $IM_{c50\%}$ is the median IM value of capacity and β_{DSR} its dispersion due to record-to-record variability, as estimated by IDA; $\lambda(IM)$ is the hazard curve, approximated as a straight line of constant slope k in log-log coordinates:

$$\lambda(IM) \approx k_0 \cdot IM^{-k} \quad (2–6)$$

For example, EN1998 [1] stipulates values of $k = 2 – 4$ for Europe, although a more accurate value can be estimated by fitting the actual hazard curve of the site at hand [22].

To incorporate the effect of additional uncertainty into Equation (2–4) we shall make the well-known first-order assumption, whereby uncertainties only act to increase the dispersion of the fragility without changing its median. Assuming a lognormal distribution, this is essentially equivalent to taking the median capacity $IM_{C50\%}$ as a random variable with a lognormal distribution having a median of 1.0 and a dispersion of β_{DSU}. Then, the x% value, $x \in [0.5,1)$, of the MAF of DS can be estimated as (Cornell et al. [20]):

$$\lambda_x(DS) \approx \lambda(DS) \exp\left(-kK_x \beta_{DSU}\right) \quad (2–7)$$

where K_x is the standard normal variate corresponding to x, $K_x = \Phi^{-1}(x)$, and $\Phi(\cdot)$ is the standard normal cumulative distribution function. For example, for $x = 84\%$, $K_x = 1$, while $x = 90\%$ yields $K_x = 1.28$. Equation (2–7) can be applied to modify $\lambda(DS)$ regardless of whether it is estimated through the closed-form solution of Equation (2–5) or the integral of Equation (2–3).

Alternatively, one can perform the estimation in a much more accurate way by directly modifying the fragility function. This approach is based on the fact that $IM_{C50\%}$ and $\lambda(DS)$ are monotonically related, whereby decreasing the median IM capacity increases the MAF. This may become more evident by inspecting Equations (2–5) and (2–6). Then, the $(1-x)$% quantile value of the median IM capacity simply corresponds to the x% value of the MAF. In other words, if a lognormal assumption has been adopted for the distribution of IM_C, then one can simply maintain the dispersion of β_{DSR}, and reduce the median $IM_{C50\%}$ to account for uncertainty:

$$IM_{C50\%}^{x} = IM_{C50\%} \exp\left(-K_x \beta_{DSU}\right) \quad (2–8)$$

Alternatively, to avoid any assumptions of lognormality, one can also directly modify the individual samples of IM_{Ci} derived from each record and IDA curve:

$$IM_{Ci}^{x} = IM_{Ci} \exp\left(-K_x \beta_{DSU}\right) \quad (2–9)$$

By employing the above modified values of IM_{Ci} capacities, one can directly derive the $(100-x)$% estimate of the fragility function $P_{1-x}[D > C|IM]$ employing his/her method of choice. By substituting this into Equation (2–3), the x% estimate of the MAF is calculated:

$$\lambda_x(DS) = \int_{IM} P_{1-x}[D > C|IM] \left|d\lambda(IM)\right| \quad (2–10)$$

Regardless of the method of computation, verification of the MAF vis-à-vis the target value of λ_{DSlim} is performed by comparing the safety margin ratio, MR, vis-à-vis the minimum allowable value of 1.0 as follows:

$$MR = \frac{\lambda_{DSlim}}{\lambda_x(DS)} > 1 \quad (2–11)$$

Ideally, the perfect q-value will correspond to $MR = 1$ for all buildings and sites. Obviously, this cannot be the case with a simple constant q-value assumption adopted by the code. At best, one can require that all sites and archetypes satisfy Equation (2–11). A less strict requirement would be to allow for the exception of a small percentage of say 5-10% of cases that would not perfectly satisfy the check, assuming this does not translate to a specific site or type of buildings being consistently unsafe.

When a given verification fails, or, even if it passes by a wider than needed margin, one would want to modify the value of q and return to Step 2 to redesign and reassess the archetypes until reasonable convergence is achieved. In such cases, similarly to Newton-Raphson iterations for solving a nonlinear equation, some estimate of a new trial q-factor value is needed. This can be easily achieved through the approximations of Cornell et al. [20]. Let q_{cur} be the current, unsatisfactory, value of q and q_{new} the new one, while $IM_{C50\%,\mathrm{cur}}$ and $IM_{C50\%,\mathrm{new}}$ are the corresponding median IM capacities. Then, the MAF of the critical *DS* can be approximated via Equation (2–7) as

$$\lambda_{x,cur}(DS) = k_0 \left(IM_{C50\%,cur}\right)^{-k} \exp\left(0.5k^2\beta_{DSR}^2 - kK_x\beta_{DSU}\right) \tag{2–12}$$

Ideally, we would want MR = 1, which, assuming the same hazard function and fragility dispersions β_R, β_U, translates to:

$$\lambda_{DSlim} = \lambda_{x,new}(DS) = k_0 \left(IM_{C50\%,new}\right)^{-k} \exp\left(0.5k^2\beta_{DSR}^2 - kK_x\beta_{DSU}\right) \tag{2–13}$$

By dividing Eq. (2–12) by (2–13) we get

$$\frac{\lambda_{x,cur}(DS)}{\lambda_{DSlim}} = \left(\frac{IM_{C50\%,cur}}{IM_{C50\%,new}}\right)^{-k} \tag{2–14}$$

In general, the lower the q, the higher the capacity becomes. For simplicity, let us assume that the median IM capacity is inversely proportional to q. Then Equation (2–14) becomes

$$\frac{\lambda_{x,cur}(DS)}{\lambda_{DSlim}} = \left(\frac{q_{new}}{q_{cur}}\right)^{-k} \Rightarrow \frac{q_{new}}{q_{cur}} = \left(\frac{\lambda_{x,cur}(DS)}{\lambda_{DSlim}}\right)^{-1/k} \Rightarrow$$

$$q_{new} = q_{cur}\left(MR_{cur}\right)^{1/k} \tag{2–15}$$

where MR_{cur} is the value of the margin ratio estimated with the current value of q_{cur}. Each failing, or suboptimal, check for a site-building combination can provide a new potential value of q_{new}. Taking the mean or some other percentile of such target values can provide the next trial q-value. Obviously, any such value would have to be rounded to within 0.5 of an integer, to be compatible with current code practice. After all, values with more significant digits would imply an accuracy that does not really exist when considering the size our archetype/site sample versus the population of all sites and buildings in Europe. Thus, given a good initial guess, one should expect a rapid convergence within one or two iterations.

As a final note, it is important to stress that the q-factors vetted by this approach already incorporate the overstrength Ω. Similar to what has been done for, e.g., moment-resisting frames in EN1998, one may opt to separate the effect of overstrength and allow tuning it on a case-by-case basis via a static pushover analysis, or permanently incorporate it. In the former case, the q-factor should be divided by the value of Ω estimated in Step 4 and appropriate guidance should be provided vis-à-vis limitations and required system characteristics so that the user can safely re-introduce it when needed.

3 Verification example

An example will be presented to showcase the verification of the q-factor currently prescribed by EN1998 for the design of DCH concentrically-braced frames (CBFs). It should be noted that the proposed approach adopts a consistent risk-basis, whereby performance objectives are prescribed in terms of the MAF of exceeding specific limit-states, effectively assigning risk at the output response. Instead, EN1998 prescribes risk at the input level via the design spectrum MAF of 10% in 50yrs, introducing considerable uncertainty in the actual performance achieved. Thus, when verifying q-factors one should take care to appropriately select the MAFs and confidence levels in the INNOSEIS approach so as to achieve levels of risk that are similar to those currently implied in EN1998. Therefore, for reasons of calibration in a normative assessment, several such studies of traditional EN1998 systems shall need to be undertaken.

3.1 Step 1: Site Hazard

For the case at hand, we are only interested in the DCH q-factors, therefore only the INNOSEIS high-seismicity sites and the corresponding hazard estimates and record set are used. The unscaled response spectra of both sets appear in Figure 3-1. By contrasting Figure 3-1(a) and Figure 3-1(b), it should become apparent that there is a distinct difference in the spectral shape of the two types of motions, with high-seismicity motions generally being more intense in moderate to long periods.

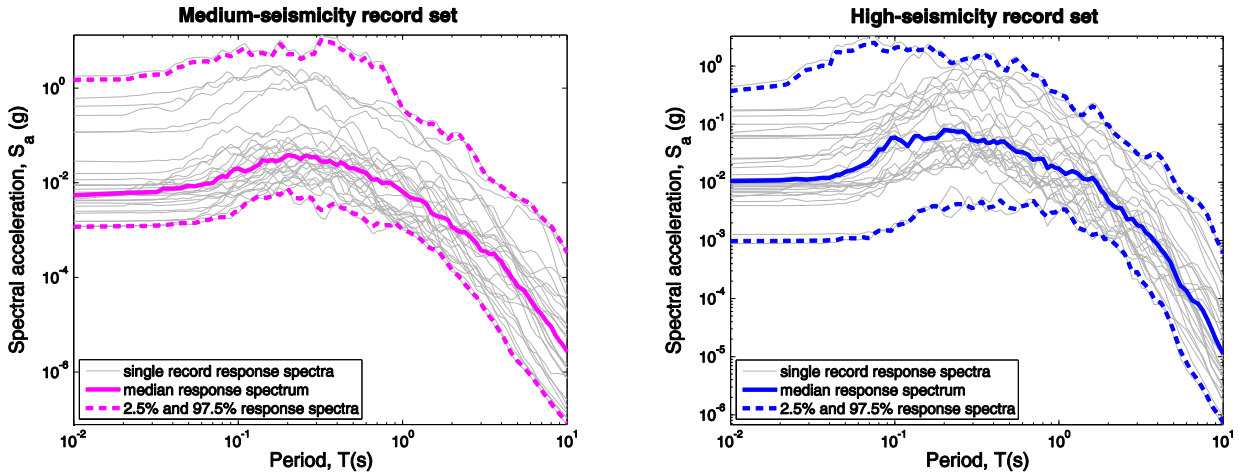

(a) (b)

Figure 3-1: Unscaled response spectra for the INNOSEIS record sets: (a) medium-seismicity, (b) high-seismicity.

3.2 Step 2: Concentrically-Braced Frame Archetypes

In order to support the methodology outlined in Chapter 2, two steel buildings, 3 and 6-storeys high, are employed. These structures have a storey-height equal to 3.5m, a bay-length of 9.0m, and cover a plan-view area of 36x54m^2 as shown in Figure 3-2. The lateral load-resisting system consists of concentrically X-braced frames (X-CBFs), where each brace extends between two consecutive floors. Composite beams are considered to support the concrete slab on each level, whereby connection with the pin-supported columns is established through bolted (shear) connections. The gravity loads considered regarding the top as well as the intermediate floors are summarised in Table 3-1. The seismic design has been performed in ETABS [23] using response spectrum analysis, following the Eurocode 8 [1] provisions for ductility class high (DCH) and a peak ground acceleration (PGA) of a_g = 0.24g. A behaviour factor q = 4 is adopted, and the soil properties on site are assumed to match the Eurocode 8 class B soil type, thus implying a soil amplification factor S = 1.2 (Figure 3-3). The steel grade that has been used is S355.

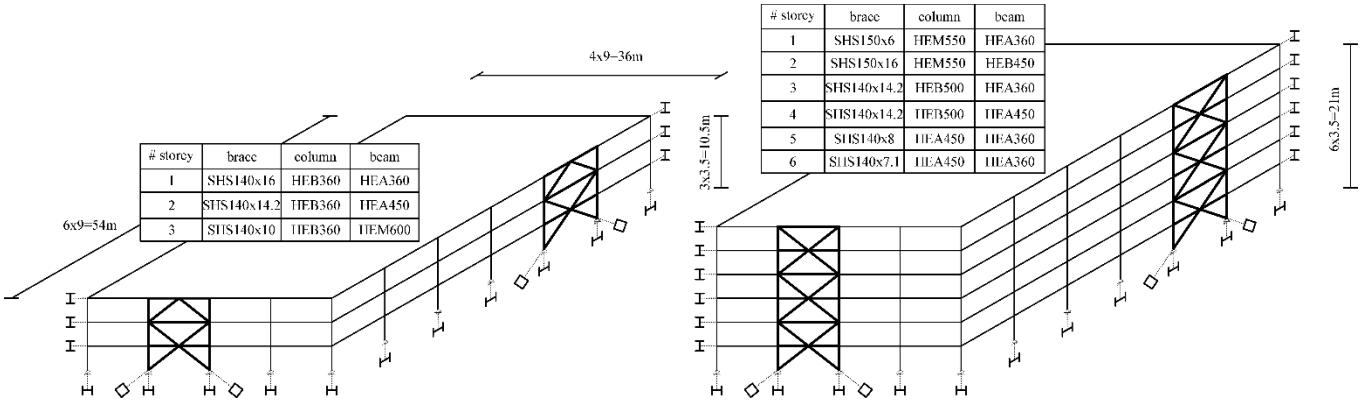

# storey	brace	column	beam
1	SHS140x16	HEB360	HEA360
2	SHS140x14.2	HEB360	HEA450
3	SHS140x10	HEB360	HEM600

# storey	brace	column	beam
1	SHS150x6	HEM550	HEA360
2	SHS150x16	HEM550	HEB450
3	SHS140x14.2	HEB500	HEA360
4	SHS140x14.2	HEB500	HEA450
5	SHS140x8	HEA450	HEA360
6	SHS140x7.1	HEA450	HEA360

Figure 3-2:Case study design-basis CBFs and member cross sections on the X-brace bays

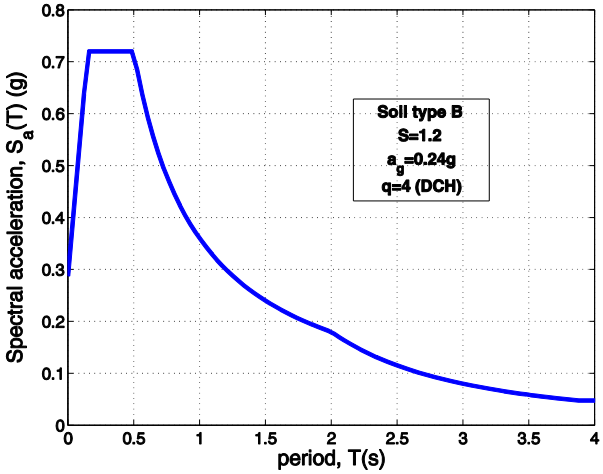

Figure 3-3: Elastic design spectrum

Table 3-1: Gravity loads considered

	i^{th} storey	Rooftop
Concrete slab	3.11kN/m^2	3.11kN/m^2
Additional dead loads	1.8kN/m^2	0.9kN/m^2
Live loads	2kN/m^2	2kN/m^2

3.3 Step 3: Nonlinear Models

Modelling-wise, all braces are taken into account by appropriately modelling their tensile and compressive behavior. Brace-frame as well as beam-column connections are considered to be rotationally flexible, while columns themselves are assumed fixed to the ground due to the effect that the rather stiff connection gusset plates are expected to have locally, despite the initial design-basis assumption for pinned support conditions (Figure 3-4). Gravity loads (Table 3-1) are introduced to the model through a leaning column that carries 50% of the vertical loads acting on the structure due to plan-view symmetry. The cross-braces are modelled using a physics-based approach [24,25], by applying an initial imperfection equal to $L/250$ on the midpoint of each member representing a brace, where L is the effective element length.

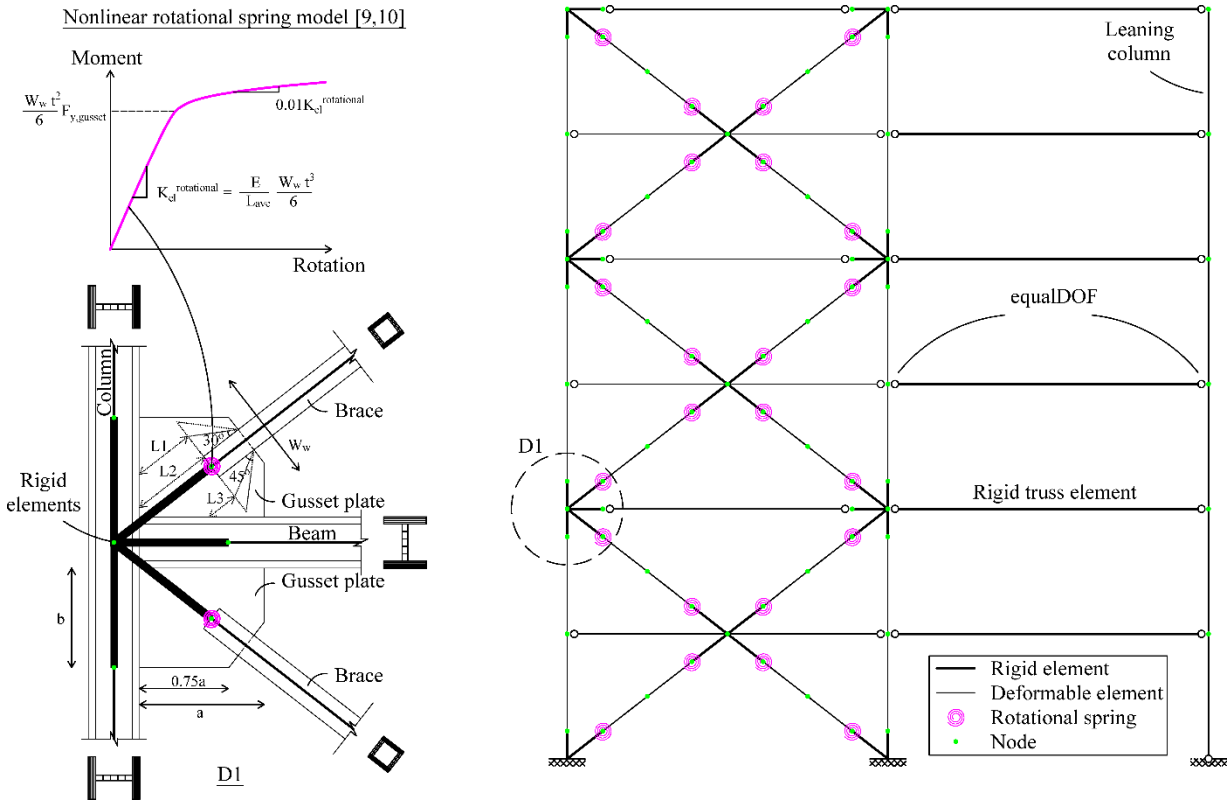

Figure 3-4: Structural model considered

Nonlinear force-based beam-column fibre elements are adopted to model braces, beams and columns of the CBF, while elastic beam-column elements are used for the leaning column. In all cases, the Steel02 material [26] from the OpenSees [27] library is adopted, using a steel Young's modulus E=210GPa, the expected yield strength f_y=1.2·355=426MPa, a post-yield hardening ratio α_h=0.3% and parameters that control the transition from elastic to plastic branches, i.e. R_0=20, c_{R1}=0.925 and c_{R2}=0.15. The hysteretic-behaviour parameters a_1=0.0005, a_2=0.01, a_3=0.0005 and a_4=0.01 are taken into account according to the Uriz and Mahin [25] approach. On top of Steel02, the OpenSees fatigue material [27] is also considered for the braces, in order to account for any potential fatigue-related failure due to cyclic loading.

Diaphragm rigidity representing the concrete slab is taken into account through stiff truss elements that connect all nodes in a floor. Convergence issues stemming from the buckling of braces are resolved using (additional) truss elements of marginal stiffness. P-Δ geometric transformation is considered for all beams and columns (leaning column included), while the corotational transformation is preferred for the braces as it is suitable for large-displacement-small-strain problems. As far as the modelling of the brace-frame connections is concerned, the out-of-plane bending of the steel gusset plate is considered. The effect of the connection flexibility, both for the brace-column and the brace-beam connections, is taken into account through nonlinear zero-length rotational springs, the properties of which are estimated based on the relationships proposed by Hsiao et al. [28,29] as shown in Figure 3-4.

Modal analysis is initially performed for both case studies to determine the fundamental period of vibration (T_1) as well the associated mass participation ratio. Although this task is trivial compared to the nonlinear analysis presented later in this section, it is necessary not only because it provides information (e.g. T_1) that will be exploited during the post-processing of the nonlinear-analysis results, but also due to the verification of the OpenSees model against the ETABS model that has been used during the design of the case studies. According to Table 3-2, some discrepancies are evident among the two approaches. In general, the OpenSees model is stiffer due to rigid-links that reduce the element length, as well as the non-pinned hinges in place of the pinned ones employed in ETABS, as per standard engineering practice.

Table 3-2: Modal analysis results; OpenSees versus ETABS

	OpenSees		ETABS	
Number of storeys	Fundamental period T_1(s)	Mass participation ratio (%)	Fundamental period T_1(s)	Mass participation ratio (%)
3	0.55	83.00	0.84	86.80
6	1.15	75.00	1.65	79.43

3.4 Step 4: Static Analysis

Nonlinear static analysis is executed in order to obtain a first guess regarding the actual behaviour factor of the case studies under investigation. A piece-wise linear fit is performed on each pushover curve in coordinates of base shear V versus roof drift θ_{roof} (or the maximum interstory drift θ_{max}) to derive the approximate first yield point (θ_y, $V_{b,y}$), the peak response (θ_{peak}, $V_{b,peak}$) and the ultimate capacity point (θ_u, $V_{b,u}$) that corresponds to a 20% drop of the system's strength (i.e. $V_{b,u} = 0.8V_{b,peak}$). An approximate behaviour factor may then be estimated as $q_{stat} = q_d \cdot \Omega = \theta_u/\theta_y \cdot V_{b,peak}/V_{b,y}$. Extracting the associated values from Figure 3-5(a) provides the behaviour factor for the 3-storey X-CBF of $q_{stat,3} \approx 10.0$, if θ_{roof} is used as a basis and $q_{stat,3} \approx 19$ for θ_{max}. Similarly, the values of Figure 3-5(b) result in the 6-storey X-CBF behaviour factor $q_{stat,6} \approx 10.8$ or 11 for θ_{roof} and θ_{max}, respectively. Obviously the static pushover is not able to accurately estimate the q-factor, as it does not incorporate risk, yet at this point it can help us validate our model and at least state that the lower design q-factor adopted is deemed acceptable vis-à-vis the much higher ductility observed in the pushover. Then, the verification process may advance to the q-factor evaluation using dynamic analysis results.

To aid in the establishment of performance criteria for Step 6, two additional (capacity) points are depicted on the pushover curve, namely the "1st element to yield" and "1st element to exceed the SD capacity". Although the former is quite simple to capture by looking for the axial strain that exceeds the associate yield (ε_y) on an element basis, the latter is triggered upon the exceedance of an axial strain value (ε_{LS}) that equals 75% of the ultimate/fracture strain (ε_u), according to the rules described in Section 2.6 (see Figure 2-14(b)), and will further be adopted for the assessment of the behaviour factor using nonlinear dynamic analysis:

$$\varepsilon_{LS} = 0.75\varepsilon_u \tag{3–1}$$

Ideally ε_u should be estimated via a series of experimental tests or through corresponding empirical or regression equations. For the purpose of this study, ε_u is estimated indirectly using the equation proposed by Hsiao et al. [29] for the maximum strain-range (ε_{range}).

$$\max\left(\varepsilon_{range}\right) = 0.1435\left(\frac{w}{t}\right)^{-0.4}\left(\frac{kL}{r}\right)^{-0.3}\left(\frac{E}{f_y}\right)^{0.2} \tag{3–2}$$

ε_{range} is the sum of the maximum absolute values of compressive and tensile strains encountered during the loading history; w/t refers to the class, kL/r to the slenderness and E/f_y to the actual (herein the expected) steel yield strength of the brace section. During an earthquake, the brace is assumed to be subjected to equal tensile and compressive strain values, and thus ε_u is assumed to be approximately equal to 50% of ε_{range}.

$$\varepsilon_u = \frac{\max\left(\varepsilon_{range}\right)}{2} \tag{3–3}$$

Limiting strain (ε) values may be translated into interstorey drift (θ) estimates either by recording corresponding values of ε and θ in the model response or by adopting a simple approximation:

$$\theta = \frac{\varepsilon\, L_{brace}}{H_{storey}\cos\varphi} \tag{3–4}$$

L_{brace} is the brace length, H_{storey} the storey height and φ the angle defined by the brace and the

horizontal. According to Figure 3-5, the simplified solution of Equation (3–4) provides similar results to the strain-based approach for each element regarding the 1st yield, typically appearing following the onset of buckling on the 1st brace. Table 3-3 summarises the 'Significant Damage' and 'Global Collapse' limit states in terms of strain and maximum inter-storey drift. These values are derived from Equations (3–3) and (3–4), and can be considered to be relatively large. A more conservative estimate would reduce the wide margins of safety appearing in Step 7.

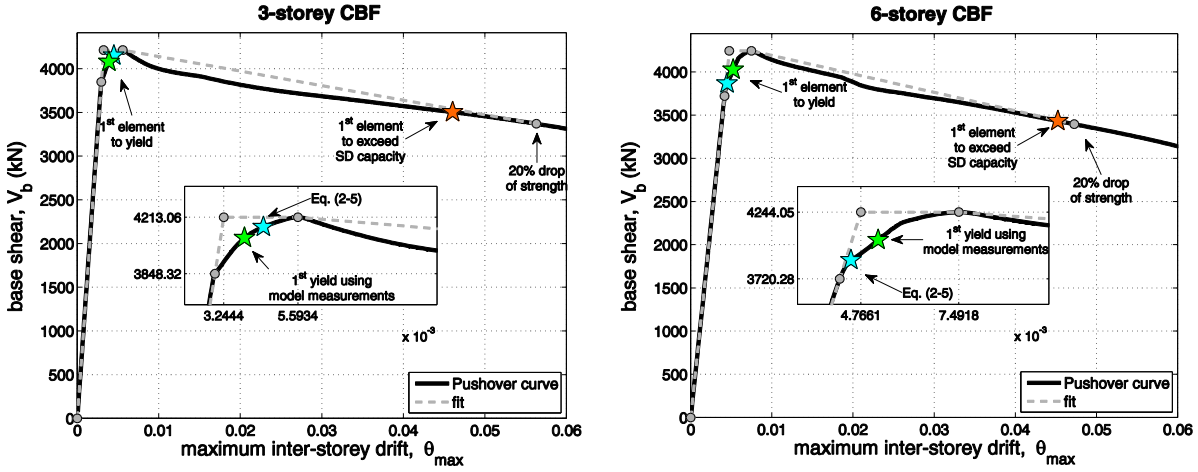

(a) (b)

Figure 3-5: Nonlinear Static Analysis: (a) 3-storey CBF, (b) 6-storey CBF

Table 3-3: Limit state capacities in terms of strain and maximum inter-storey drift

	Limit State	ε (%)	θ_{max} (%)
3-storey	LS	2.97	4.60
	GC	+∞	+∞
6-storey	LS	2.92	4.52
	GC	+∞	+∞

3.5 Step 5: Dynamic Analysis

IDA is subsequently performed to derive a refined representation of the relationship among engineering demand parameters (*EDPs*) of interest and the ground motion intensity measure (*IM*) that will eventually be exploited for the robust assessment of the behaviour factor. For the purpose of this study, the maximum inter-storey drift ratio (i.e. θ_{max}) is adopted as the *EDP* and the average spectral acceleration ($AvgS_a$) shown in Eq. (2–1) as a state-of-the-art *IM*. The IDA output for both case studies is presented in Figure 3-6.

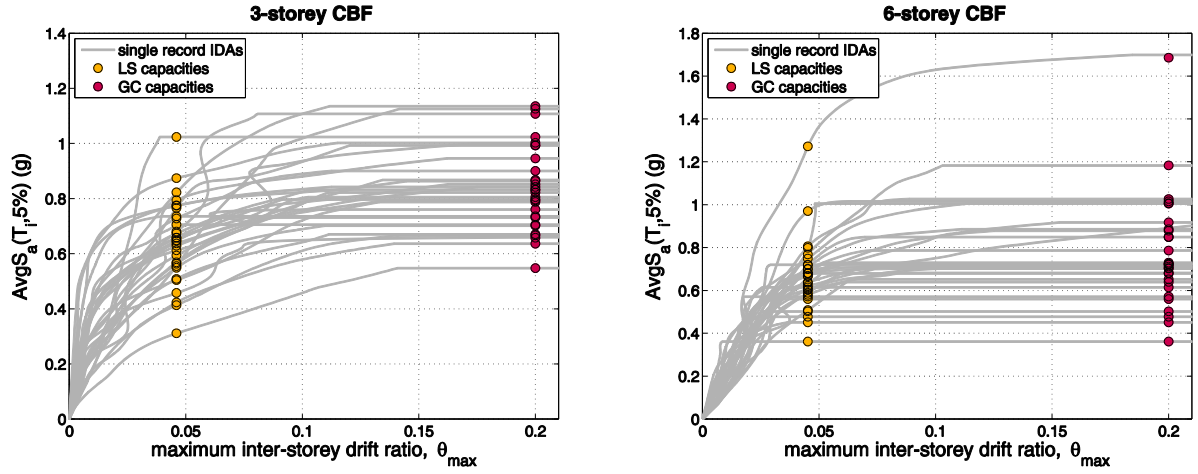

(a) (b)

Figure 3-6: Single record IDAs along with the associated LS and GC capacities: (a) 3-storey CBF, (b) 6-storey CBF

3.6 Step 6: Performance Criteria and Fragility Assessment

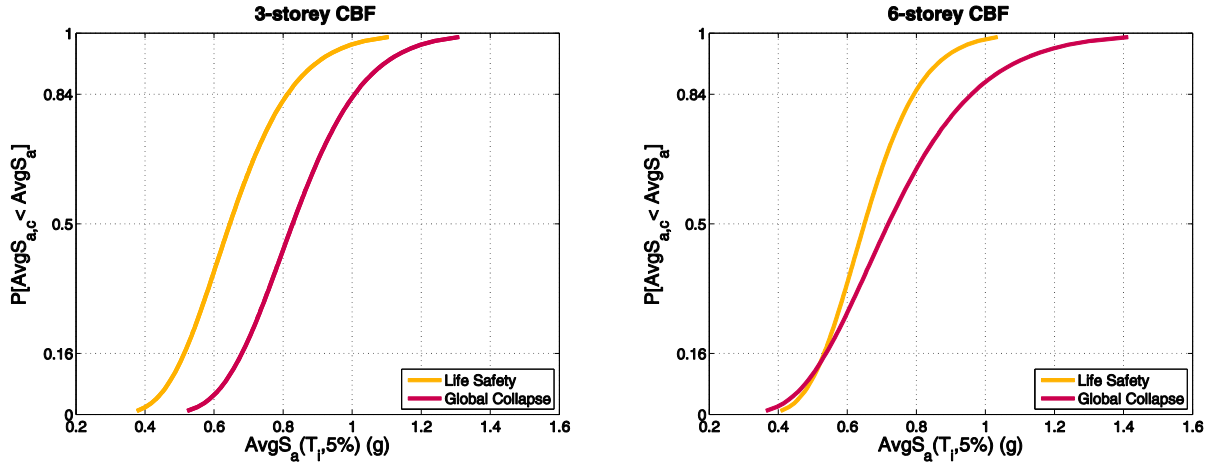

(a) (b)

Figure 3-7: LS and GC fragility curves: (a) 3-storey CBF, (b) 6-storey CBF

Having such information on the structural response at our disposal enables the accurate probability of exceedance estimation for any of the limiting criteria defined above (Table 3-3). The estimation may simply be performed by considering a vertical cut (or *EDP* stripe) of the IDA plane on each *EDP* capacity of interest (e.g. for LS, GC). Interpolating the single-record IDA curves at the designated θ_{max} capacity results in vertical stripes of the so-called *IM*-capacities, or in other words the values that define the damage state distribution. Such information is conveniently summarized using the well-known fragility curves presented in Figure 3-7. Therein, the conditional probability of violating the aforementioned limit state capacities is provided for all values of seismic intensity.

3.7 Step 7: Acceptance or rejection of q-factor

The seismic fragility output of Figure 3-7 is convolved with the seismic hazard curves appearing in Figure 2-15 for the high-seismicity sites of Athens, Perugia and Focsani. The result is the mean annual frequency of exceedance for the limit states of interest. Uncertainty dispersions of $\beta_{LSU} = 0.2$ and $\beta_{GCU} = 0.3$ are assumed, together with a moderate confidence level of $x = 80\%$. The case study MAFs of $\lambda_x(DS)$, the associated limiting values, λ_{DSlim}, and the margin ratio, $\lambda_{DSlim} / \lambda_x(DS)$, are summarized in Table 3-4 and Table 3-5 using the approximate closed-form solution of Equation (2–7) on top of Equation (2–3) and for GC objectives of 1% and 2% in 50yrs, respectively. For comparison, the same quantities are also derived with the more accurate computational approach of Equation (2–10) and appear in Table 3-6 and Table 3-7.

Comparing the margin ratio against its allowable value of 1.0 determines the acceptance or rejection of the design-basis q-factor. In our case, the results are the same regardless of the assessment approach (analytical versus numerical). For both buildings and all sites, the LS objective is easily satisfied. The same holds for GC with the sole exception of the 6-story structure in Athens under the stricter 1% in 50yrs limit. For this risk limit, the initial (design) assumption for a behaviour factor of $q = 4$ is acceptable. If we use the stricter GC limit of 1% in 50 years, then a small reduction of the q-factor is required. Despite the small sample of buildings tested, it should become obvious that EN1998 cannot guarantee a consistent risk for either LS or GC. Still, EN1998 manages to easily satisfy LS requirements, while it remains troubled by GC where the actual risk does not always comply with a strict maximum allowable MAF of 1% in 50yrs.

Table 3-4: Behaviour factor verification using the closed form solution (*x*=80%, LS at 10% in 50yrs, GC at 1% in 50yrs).

Site	Case study	Design q-factor	Limit State	$\lambda_x(DS)$ (‰)	$\lambda_{DS\text{lim}}$ (‰)	Margin Ratio (λ_{lim} / λ_x)	Check	Next iteration q-factor
Athens	3-story	4	LS	0.242	2.107	8.72	✓	-
			GC	0.116	0.201	1.73		
	6-story	4	LS	0.206	2.107	10.24	×	3.8
			GC	0.225	0.201	0.89		
Perugia	3-story	4	LS	0.127	2.107	16.55	✓	-
			GC	0.053	0.201	3.82		
	6-story	4	LS	0.126	2.107	16.73	✓	-
			GC	0.142	0.201	1.41		
Focsani	3-story	4	LS	0.016	2.107	131.44	✓	-
			GC	0.003	0.201	75.45		
	6-story	4	LS	0.008	2.107	262.88	✓	-
			GC	0.021	0.201	9.43		

Table 3-5: Behaviour factor verification using the closed form solution (*x*=80%, LS at 10% in 50yrs, GC at 2% in 50yrs).

Site	Case study	Design q-factor	Limit State	$\lambda_x(DS)$ (‰)	$\lambda_{DS\text{lim}}$ (‰)	Margin Ratio (λ_{lim} / λ_x)	Check	Next iteration q-factor
Athens	3-story	4	LS	0.242	2.107	8.72	✓	-
			GC	0.116	0.404	3.48		
	6-story	4	LS	0.206	2.107	10.24	✓	-
			GC	0.225	0.404	1.79		
Perugia	3-story	4	LS	0.127	2.107	16.55	✓	-
			GC	0.053	0.404	7.67		
	6-story	4	LS	0.126	2.107	16.73	✓	-
			GC	0.142	0.404	2.84		
Focsani	3-story	4	LS	0.016	2.107	131.44	✓	-
			GC	0.003	0.404	151.65		
	6-story	4	LS	0.008	2.107	262.88	✓	-
			GC	0.021	0.404	18.96		

Table 3-6: Behaviour factor verification via the numerical approach (*x*=80%, LS at 10% in 50yrs, GC at 1% in 50yrs).

Site	Case study	Design q-factor	Limit State	λ_x (DS) (‰)	λ_{lim} (‰)	Margin Ratio (λ_{lim} / λ_x)	Check	Next iteration q-factor
Athens	3-story	4	SD	0.286	2.107	7.370	✓	-
			GC	0.161	0.201	1.252		
	6-story	4	SD	0.246	2.107	8.553	×	3.5
			GC	0.276	0.201	0.728		
Perugia	3-story	4	SD	0.166	2.107	12.660	✓	-
			GC	0.084	0.201	2.381		
	6-story	4	SD	0.168	2.107	12.525	✓	-
			GC	0.198	0.201	1.013		
Focsani	3-story	4	SD	0.033	2.107	63.334	✓	-
			GC	0.007	0.201	28.658		
	6-story	4	SD	0.019	2.107	109.522	✓	-
			GC	0.038	0.201	5.227		

Table 3-7: Behaviour factor verification via the numerical approach (*x*=80%, LS at 10% in 50yrs, GC at 2% in 50yrs)

Site	Case study	Design q-factor	Limit State	λ_x(DS) (‰)	λ_{lim} (‰)	Margin Ratio (λ_{lim} / λ_x)	Check	Next iteration q-factor
Athens	3-story	4	SD	0.286	2.107	7.370	✓	-
			GC	0.161	0.404	2.517		
	6-story	4	SD	0.246	2.107	8.553	✓	-
			GC	0.276	0.404	1.464		
Perugia	3-story	4	SD	0.166	2.107	12.660	✓	-
			GC	0.084	0.404	4.785		
	6-story	4	SD	0.168	2.107	12.525	✓	-
			GC	0.198	0.404	2.037		
Focsani	3-story	4	SD	0.033	2.107	63.334	✓	-
			GC	0.007	0.404	57.607		
	6-story	4	SD	0.019	2.107	109.522	✓	-
			GC	0.038	0.404	10.507		

References

1. CEN. *Eurocode 8 : Design of structures for earthquake resistance - Part 1: General rules, seismic actions and rules for buildings (EN 1998-1:2004)*. vol. 1. CEN, Brussels: 2004.
2. FEMA. *Quantification of Building Seismic Performance Factors*. FEMA P-695, Prepared by Applied Technology Council for Federal Emergency Management Agency, Washington, D.C.: 2009.
3. Giardini D, Woessner J, Danciu L, Crowley H, Cotton F, Grünthal G, *et al.* Seismic Hazard Harmonization in Europe (SHARE): Online Data Resource 2013. DOI: 10.12686/SED-00000001-SHARE.
4. Cordova P, Deierlein G, Mehanny SF, Cornell CA. Development of a two-parameter seismic intensity measure and probabilistic design procedure. *The Second U.S.- Japan Workshop on Performance-Based Earthquake Engineering Methodology for Reinforced Concrete Building Structures*, Sapporo, Hokkaido: 2001.
5. Vamvatsikos D, Cornell CA. Developing efficient scalar and vector intensity measures for IDA capacity estimation by incorporating elastic spectral shape information. *Earthquake Engineering and Structural Dynamics* 2005; **34**(13): 1573–1600. DOI: 10.1002/eqe.496.
6. Kazantzi AK, Vamvatsikos D. Intensity measure selection for vulnerability studies of building classes. *Earthquake Engineering & Structural Dynamics* 2015; **44**(15): 2677–2694. DOI: 10.1002/eqe.2603.
7. Lin T, Haselton CB, Baker JW. Conditional spectrum-based ground motion selection. Part I: Hazard consistency for risk-based assessments. *Earthquake Engineering & Structural Dynamics* 2013; **42**(12): 1847–1865. DOI: 10.1002/eqe.2301.
8. Lin T, Haselton CB, Baker JW. Conditional spectrum-based ground motion selection. Part II: Intensity-based assessments and evaluation of alternative target spectra. *Earthquake Engineering & Structural Dynamics* 2013; **42**(12): 1867–1884. DOI: 10.1002/eqe.2303.
9. Kohrangi M, Vamvatsikos D, Bazzurro P. Site dependence and record selection schemes for building fragility and regional loss assessment. *Earthquake Engineering & Structural Dynamics* 2017(i). DOI: 10.1002/eqe.2873.
10. Kohrangi M, Bazzurro P, Vamvatsikos D, Spillatura A. Conditional spectrum-based ground motion record selection using average spectral acceleration. *Earthquake Engineering & Structural Dynamics* 2017; **44**: 657–675. DOI: 10.1002/eqe.2876.
11. Kohrangi M, Vamvatsikos D. INNOSEIS ground motion set for high seismicity European sites 2016. http://innoseis.ntua.gr/high_record_set.rar.
12. Kohrangi M, Vamvatsikos D. INNOSEIS ground motion set for medium seismicity European sites 2016. http://innoseis.ntua.gr/medium_record_set.rar.
13. CEN. *Eurocode 3 : Design of steel structures - Part 1: General rules and rules for buildings (EN 1993-1:2005)*. CEN, Brussels: 2005.
14. Vamvatsikos D, Cornell CA. Incremental dynamic analysis. *Earthquake Engineering & Structural Dynamics* 2002; **31**(3): 491–514. DOI: 10.1002/eqe.141.
15. Kohrangi M, Bazzurro P, Vamvatsikos D. Vector and Scalar IMs in Structural Response Estimation: Part II – Building Demand Assessment. *Earthquake Spectra* 2016; **53**(9). DOI: 10.1193/053115EQS081M.
16. Vulcu C, Stratan A, Ciutina A, Dubina D. Beam-to-CFT High-Strength Joints with External Diaphragm. I: Design and Experimental Validation. *Journal of Structural Engineering* 2017; **143**(5): 4017001. DOI: 10.1061/(ASCE)ST.1943-541X.0001709.

17. ASCE. *Seismic Evaluation and Retrofit of Existing Buildings*. Reston, VA: American Society of Civil Engineers; 2014. DOI: 10.1061/9780784412855.
18. FEMA. *Quantification of Building Seismic Performance Factors: Component Equivalency Methodology*. FEMA P-795, Prepared by Applied Technology Council for Federal Emergency Management Agency and ATC Management and Oversight, Washington, D.C.: 2011.
19. FEMA. *Prestandard and Commentary for The Seismic Rehabilitation of Buildings*. FEMA-356, Prepared by the Building Seismic Safety Council for the Federal Emergency Management Agency, Washington, D.C.: 2000.
20. Cornell CA, Jalayer F, Hamburger RO, Foutch D. Probabilistic Basis for 2000 SAC Federal Emergency Management Agency Steel Moment Frame Guidelines. *Journal of Structural Engineering* 2002; **128**(4): 526–533. DOI: 10.1061/(ASCE)0733-9445(2002)128:4(526).
21. FEMA. *Seismic Performance Assessment of Buildings*. vol. 1. FEMA P-58, Prepared by the Applied Technology Council for the Federal Emergency Management Agency, Washington D.C: 2012.
22. Vamvatsikos D. Accurate Application and Second-Order Improvement of SAC/FEMA Probabilistic Formats for Seismic Performance Assessment 1. *Journal of Structural Engineering* 2014; **140**(2): 4013058. DOI: 10.1061/(ASCE)ST.1943-541X.0000774.
23. Computers & Structures Inc. ETABS 2015.
24. Uriz P, Filippou FC, Mahin SA. Model for Cyclic Inelastic Buckling of Steel Braces. *Journal of Structural Engineering* 2008; **134**(4): 619–628. DOI: 10.1061/(ASCE)0733-9445(2008)134:4(619).
25. Uriz P, Mahin S a. *Toward Earthquake-Resistant Design of Concentrically Braced Steel-Frame Structures*. PEER Report No. 2008/08, Pacific Earthquake Engineering Research Center, University of California, Berkeley, CA: 2008.
26. Menegotto M, Pinto PE. *Method of analysis for cyclically loaded R .C. plane frames including changes in geometry and non-elastic behaviour of elements under combined normal force and bending*. Preliminary Report IABSE, Vol 13: 1973.
27. McKenna F, Fenves GL. The OpenSees Command Language Manual (1.2 edn) 2001.
28. Hsiao PC, Lehman DE, Roeder CW. Improved analytical model for special concentrically braced frames. *Journal of Constructional Steel Research* 2012; **73**(2012): 80–94. DOI: 10.1016/j.jcsr.2012.01.010.
29. Hsiao PC, Lehman DE, Roeder CW. A model to simulate special concentrically braced frames beyond brace fracture. *Earthquake Engineering & Structural Dynamics* 2013; **42**(2): 183–200. DOI: 10.1002/eqe.2202.

List of Figures

List of Tables